Stochastic Resonance in Thermally Bistable Josephson Weak Links and Micro-SQUIDs

Sagar Paul,[1] Ganesh Kotagiri,[1] Rini Ganguly,[2] Hervé Courtois,[2] Clemens B. Winkelmann,[2] and Anjan K. Gupta[1,*]

[1] *Department of Physics, Indian Institute of Technology Kanpur, Kanpur 208016, India*
[2] *Univ. Grenoble Alpes, CNRS, Grenoble INP, Institut Néel, Grenoble 38000, France*

(Received 23 October 2020; revised 3 January 2021; accepted 14 January 2021; published 3 February 2021)

Constriction-based Josephson weak links display a thermal bistability between two states exhibiting zero and finite voltages. This manifests in experiments either as hysteresis in the current-voltage characteristics of weak links or as a random telegraphic signal in voltage. In the latter case, a noise-driven amplification of a sinusoidal excitation of the device is observed, at frequencies matching the characteristic switching frequency in the telegraphic signal, a phenomenon known as stochastic resonance. The observed behavior is understood using a two-state model of stochastic resonance and is exploited to illustrate an enhanced signal-to-noise-ratio in a μ-SQUID as a magnetic field sensor.

DOI: 10.1103/PhysRevApplied.15.024009

I. INTRODUCTION

Periodically driven bistable systems exhibit an enhanced response when the noise-induced stochastic transition rate between the two states of the bistable system matches with the drive frequency. This is the phenomenon of stochastic resonance (SR) that was first invoked as a plausible explanation for the periodic occurrence of "ice ages" [1,2]. It has since been studied in several bistable systems, including electronic circuits [3], mesoscopic electronic systems [4,5], lasers [6], semiconductor devices [7], nanomechanical oscillators [8], particle traps [9], chemical systems [10], as well as in superconducting quantum interference devices (SQUIDs) having bistability with respect to magnetic flux [11,12].

The random switching of a bistable system between two states leads to a random telegraphic noise (RTN) in a suitable measured quantity. The power spectral density of this RTN has a Lorenzian shape [13] with a cutoff frequency f_c determined by Kramer's rate [14]. The latter is characteristic of the switching between the two states. It depends both on the noise intensity and the energy barrier height between the two stable states. The phenomenon of stochastic resonance consists of a peak in the response to a periodic drive, as a function of the noise-controlled cutoff frequency f_c, when it matches the drive frequency. Thus there exists an optimum noise level that enhances the system response to an excitation [15].

Josephson weak links (WLs) based on a constriction between two superconductors have been of interest for their physics [16] and applications, such as radiation detectors [17] and nanoscale magnetometry [19] using micron-size SQUID, i.e., μ-SQUID [19,22]. Thus, a better understanding of these WLs is essential for further improvements in such devices. Constriction-based superconducting weak links exhibit a dynamic thermal bistability [23,24], in addition to the static thermal bistabilities [22,25]. The former, of interest here, exists in certain bias current I_b range, starting from the dynamic retrapping current I_r^{dyn} and up to the critical current I_c. The two possible WL states in this current range are the superconducting, zero-voltage state and the dissipative, nonzero voltage state. Well above a certain threshold temperature T_h, a rapid switching between these two states leads to the disappearance of hysteresis and observation of an average intermediate voltage. In a μ-SQUID, with two WLs in parallel forming a micron-scale loop, this enables the detection of a highly flux-sensitive voltage for magnetometry operation. This voltage-readout mode [23] has advantages in terms of speed and sensitivity as compared to the more commonly used critical current measurement in a current-sweep mode [19] in hysteretic devices. As the temperature is lowered, the switching frequency decreases, leading to an observable RTN in the WL voltage [26], before eventually entering the fully hysteretic state well below T_h.

In this paper, we explore the transition of thermally bistable superconducting weak links from a reversible regime towards a hysteretic regime. We observe random switching between two voltage states with a Lorenzian frequency spectrum whose cutoff frequency increases with temperature. Furthermore, ac driving at frequencies up to

*anjankg@iitk.ac.in

 © 2021 American Physical Society

this cutoff frequency leads to a relatively large magnitude deterministic signal with an enhanced signal-to-noise ratio. These observations are quantitatively understood using a two-state model [6] of stochastic resonance. This enables us to demonstrate an enhanced signal-to-noise-ratio in a μ-SQUID magnetic field sensor in a certain operating regime.

II. BISTABILITY, RANDOM TELEGRAPHIC NOISE, AND STOCHASTIC RESONANCE

Random telegraphic noise appears in systems exhibiting two (meta)stable states $i = 1, 2$, separated by an energy barrier, as depicted in Fig. 1 inset, when exposed to a white noise of intensity D. The latter can arise from thermal fluctuations or any other noise source. The system will switch randomly from state i to the other at the classical Kramer rate [14], $r_i = (\omega_i\omega_b/2\pi\gamma)\exp(-\Delta U_i/D)$. Here, ΔU_i is the barrier height seen from the state-i minimum, γ is the viscous friction, and ω_i^2, ω_b^2 are proportional to the second derivative of the potential at the corresponding potential minimum and at the peak of the barrier in between two states, respectively. Thus for a fixed ΔU_i, the rate r_i will increase sharply with the noise D.

The system spends an average residency time $\tau_i \sim 1/r_i$ in state i. This leads to probabilities $p_i = \tau_i/(\tau_1 + \tau_2)$ of finding the system in state i. For the WL system under study, the instantaneous voltage V in state 1 is zero and in state 2 it is v [27]. Once averaged over a time larger than both τ_i's, it is $V_{\rm av} = p_2 v$. The standard deviation of the measured V will be given by $\sigma_V^2 = (1-p_2)V_{\rm av}^2 + p_2(V_{\rm av} - v)^2$, which on eliminating p_2 in favor of v and $V_{\rm av}$ gives

$$\sigma_V^2 = V_{\rm av}(v - V_{\rm av}). \tag{1}$$

As shown in Fig. 3(b), this quadratic dependence is accurately observed in the experiments and allows for a precise determination of the symmetric point, defined by $\tau_1 = \tau_2 = \tau_0$, as the position of the maximum of σ_V^2.

The spectral noise density [28] of the RTN in V works out to be [13] $S_V^N(f) = 4v^2/\{(\tau_1+\tau_2)[(\tau_1^{-1}+\tau_2^{-1})^2 + (2\pi f)^2]\}$. Here, a δ-function peak at $f = 0$, corresponding to nonzero $V_{\rm av}$, is omitted. At the symmetric point we obtain [29]

$$S_V^N(f) = \frac{v^2 f_c}{2\pi(f^2 + f_c^2)}, \tag{2}$$

with the cutoff frequency $f_c = 1/\pi\tau_0$. The total noise power, integrated over all frequencies, matches with the variance $\sigma_V^2 = v^2/4$ of the symmetric case for which $V_{\rm av} = v/2$, see Eq. (1).

We elaborate further on stochastic resonance from the superconducting WL viewpoint using the two-state model of McNamara *et al.* [6,30]. In a WL, the drive parameter is the bias current I_b. When the latter deviates by a small amount δI from the symmetric value I_{b0} defined by $\tau_1 = \tau_2 = \tau_0$ (see Fig. 1 inset), this induces an imbalance of the τ_i's, which we write up to linear order in δI as $\tau_i = \tau_0(1 \mp \alpha_i\delta I)$. As Kramer's rate dependence on I_b is predominantly determined by that of ΔU_i, as compared to that of ω_i, we write

$$\alpha_i \approx \mp\frac{1}{D}\left[\frac{\partial\Delta U_i}{\partial I_b}\right]_{I_b=I_{b0}}. \tag{3}$$

For a bias current I_b close to the symmetric point, we get $V_{\rm av} = v\tau_2/(\tau_1+\tau_2) = (v/2)[1 + \alpha\delta I]$ with $\alpha = (\alpha_1 + \alpha_2)/2$. The slope of the dc current-voltage characteristics (IVC) at I_{b0} is thus given by $dV_{\rm av}/dI = \alpha v/2$. This parameter α, with v known from the peak value of σ_V^2, can thus be determined experimentally from a (slowly acquired) IVC.

We now consider a periodic drive $\delta I = \delta I_0\cos(2\pi f_{\rm dr}t)$ of the bias current about I_{b0}, which creates a periodic modulation in τ_i at the drive frequency $f_{\rm dr}$. We assume the drive to be small enough to perturb the potential only minutely so as not to cause any transitions by itself. We also consider the adiabatic limit: the drive frequency is kept much smaller than the intrinsic frequencies $\omega_{1,2}$, so that no transition can occur by way of deterministic dynamics. The ensemble-averaged response in the WL voltage works out [29,30] as $\langle V(t)\rangle = \frac{v}{2} + V_0\cos(2\pi f_{\rm dr}t - \theta)$ with the

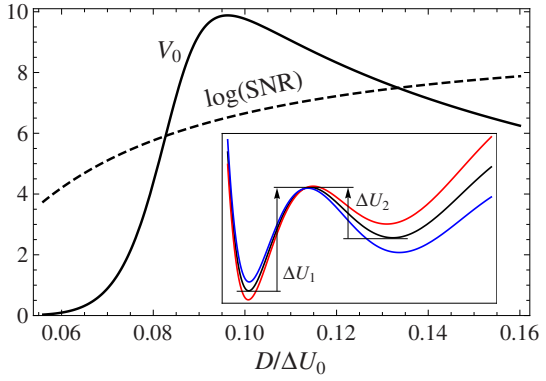

FIG. 1. Schematic variation of response V_0 to an ac current modulation and corresponding log(SNR) as a function of noise intensity D. The continuous line shows $(\Delta U_0/D)[1 + (f_{\rm dr}/f_c)^2]^{-1/2}$ for V_0 and dashed line shows $\log_{10}[(\Delta U_0/D)^2 f_c]$ for log(SNR) with $f_c = f_0\exp(-\Delta U_0/D)$. Here, $f_0 = 10^7$ Hz and $f_{\rm dr} = 100$ Hz. The inset shows a schematic of the energy corresponding to the bias currents: I_{b0} (black), $I_{b0} - \delta I$ (red), $I_{b0} + \delta I$ (blue). $\Delta U_{1,2}$, marked for the black curve corresponding to the symmetric case for a given D, define the two barrier energies.

amplitude V_0 given by

$$V_0 = \delta I_0 \frac{\alpha v}{2} \sqrt{\frac{{f_c}^2}{f_{\rm dr}^2 + {f_c}^2}}. \quad (4)$$

Here, the phase θ follows $\tan\theta = f_{\rm dr}/f_c$. The maximum response occurs at small frequencies $f_{\rm dr} \ll f_c$ with a magnitude $V_0(f_c, 0) = \delta I_0(\alpha v/2)$, i.e., the slope of the IVC times the current modulation amplitude. The voltage response is similar to a second-order low-pass filter with a bandwidth limited by the cutoff frequency f_c. The overall power spectral density in V is [30]

$$S_V(f) = [1 - (2V_0^2/v^2)]S_V^N(f) + (V_0^2/2)\delta(f - f_{\rm dr}). \quad (5)$$

Compared to the equilibrium state with no excitation, a fraction $2V_0^2/v^2$ of the noise power gets transformed into a signal power at $f_{\rm dr}$, so that the total power still remains $v^2/4$. The SNR, defined as the ratio of the signal power to the noise power in a 1-Hz bandwidth at the signal frequency, works out as

$$R_{\rm S/N} = \frac{\pi}{4}(\alpha \delta I_0)^2 f_c. \quad (6)$$

The behavior of both the response amplitude V_0 and the SNR can be discussed qualitatively with simple assumptions. The cutoff frequency f_c increases strongly with the noise amplitude D, with a dependence in between $\exp(-\Delta U_1/D)$ and $\exp(-\Delta U_2/D)$ [31], which we assume to be $\exp(-\Delta U_0/D)$ with ΔU_0 in between ΔU_1 and ΔU_2. At the same time, the parameter α decreases with D, but only as D^{-1}, see Eq. (3). Overall, we find SNR $\propto D^{-2} f_c(D)$. The SNR thus increases with the noise intensity D. This occurs in spite of the signal magnitude reduction as the spectral density of RTN reduces faster with D than the signal. Practically, the experiments will also have noise from other sources, such as measurement electronics, and at some point the noise from other sources will dominate over that of RTN. As a result, the actual measured SNR will decrease after this point.

From Eqs. (3) and (4), we find $V_0 \propto D^{-1}[1 + \{f_{\rm dr}/f_c(D)\}^2]^{-1/2}$. The behavior of V_0 and SNR as a function of the noise amplitude $D/\Delta U_0$ and at a fixed drive frequency $f_{\rm dr}$ is displayed in Fig. 1. A peak in V_0 is observed when the cutoff frequency matches the drive frequency, i.e., $f_c = f_{\rm dr}$. A more quantitative analysis requires the detailed knowledge of the whole potential profile, including ΔU_i, ω_i, ω_b, and γ, together with its dependence on the current bias I_b.

III. THERMAL BISTABILITY IN WEAK LINKS

Let us now discuss the physics of Josephson WLs while keeping the stochastic resonance in view. A Josephson WL [16] consists of a short region concentrating the phase drop φ between two bulk superconducting condensates. It can be formed by a tunnel junction, a normal-metallic link, or simply a narrow superconducting constriction. The IVC of such WL devices often show hysteresis. During current ramp up, the voltage switches from zero to a nonzero value at the critical current I_c. During current ramp down from the finite-voltage state, hysteretic devices transit back to a zero voltage at a retrapping current less than the critical current. In the present work, the bistability refers to the zero and nonzero voltage states of the WL, whereas earlier stochastic resonance studies in SQUIDs [11,12] pertain to the bistability with respect to magnetic flux.

In tunnel-junction-based Josephson junctions, the resistively and capacitively shunted-junction (RCSJ) model [32] successfully describes the transport characteristics and other aspects of the phase φ dynamics. This model leads to a tilted-washboard potential $-(\hbar I_c/2e)(\cos\varphi + I_b/I_c)$ exhibiting minima (for $I_b < I_c$) at a $\Delta\varphi = 2\pi$ interval and a tilt proportional to the current bias I_b. The φ dynamics is then described by the motion, in this potential, of a particle with position φ, mass $(\hbar/2e)^2 C$, with C as junction capacitance, subjected to a drag-force proportional to the junction conductance. In the zero-voltage state, φ takes a static value at a potential minimum, separated by energy barriers from neighboring minima. The height of the barrier, in between two neighboring minima, reduces with increasing bias current I_b and vanishes at $I_b = I_c$. The barrier height for I_b close to I_c is given by $(\hbar I_c/2e)(1 - I_b/I_c)^{3/2}$ [32]. Any transition to a neighboring minimum, through thermal activation or quantum tunneling, amounts to a change in φ by 2π and is called a phase-slip event. Such an event leads to a voltage pulse and thus Joule heat deposition. In the nonzero-voltage steady state, φ evolves continuously with time, leading to a voltage $V = (\hbar/2e)(d\varphi/dt)$. According to this model, hysteresis arises when the C-dependent inertial term in the equation of motion for φ dominates over the drag term.

Constriction-type WLs have negligible capacitance C, or mass term in the RCSJ model, but their IVC often still show hysteresis. This is attributed to heat generated [33] by the large critical current in such WLs, hence a large dissipated power $I_c V$ at the voltage onset, together with the poor heat evacuation from such a nanoscale object. A dynamic thermal model (DTM), incorporating heating effects together with phase dynamics, describes well the bistability between the zero and finite voltage states that is found within a bias-current range $I_r^{\rm dyn} < I_b < I_c$ [24]. The so-called dynamic retrapping current $I_r^{\rm dyn}$ never exceeds the critical current I_c but the two approach zero as the bath temperature T approaches the critical temperature T_c. The extent of the bistable region in bias current, i.e., $I_c - I_r^{\rm dyn}$, decreases with increasing temperature while both states become more susceptible to noise. As a result, the

WL switches randomly between the two states above a crossover temperature T_h, leading to a random telegraphic noise in voltage.

Although one can understand the bistability using the DTM, evaluating the susceptibility of the two states to noise requires a detailed understanding of the effective potential or free energy of the WL, which is coupled to a thermal bath, and as a function of bias current. The theoretical approaches on the switching statistics of the two states in Josephson weak links due to noise are based on the tilted washboard potential [34] that ignore heating effects. In fact, there is no such general formulation of free energy for such a dissipative and open dynamical system. Qualitatively, any transition from the zero-voltage state to the dissipative state is triggered by a phase slip. However, every phase slip may not eventually lead to the steady dissipative state as it requires accumulation of more heat than that of a single phase slip [36]. Nevertheless, for the experimental results and analysis reported here, the detailed knowledge of the free energy, though insightful, is not essential for the validity of the two-state model. All the required parameters, such as the temperature-dependent α and f_c, can be extracted from the IVC and noise power spectral density.

IV. EXPERIMENTAL DETAILS

We study superconducting WL devices made of two bulklike superconductors connected by a short and narrow constriction as shown in the inset of Fig. 2(a) with two current and two voltage pads that are more than 100 μm away from the WL. These are fabricated using e-beam-evaporated 20-nm-thick films of Nb on a Si substrate by patterning an aluminum mask through electron-beam lithography and liftoff [23]. The aluminum pattern is then transferred to Nb by reactive ion etching, followed by wet aluminum removal. The patterned width of the WL is 30 nm. Four-probe electrical measurements are carried out in a 1.3-K base-temperature closed-cycle refrigerator. All the sample leads in this setup pass through a low-temperature copper powder filter and room-temperature π filter for reducing noise interference.

The measurement electronics consists of a ground-isolated current source for current bias and a commercial voltage amplifier with 100-kHz bandwidth for sample voltage amplification. The amplified voltage is digitized with electronics capable of 250 kS/s maximum sampling rate. A lock-in amplifier is used for the ac current bias and phase-sensitive ac voltage detection. An antialiasing filter with low-pass cutoff of 50 kHz and 12 dB/Octave rolloff is used after the voltage amplifier. The voltage data for spectral analysis are acquired at 100-kS/s acquisition rate. The power spectral density of voltage $S_V(f)$ is obtained from the voltage time series after mean subtraction. The reported

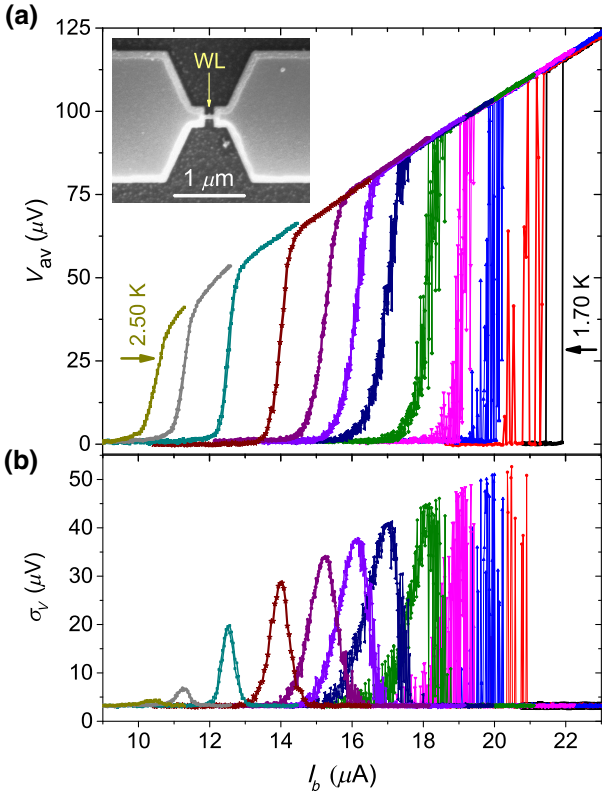

FIG. 2. (a) $V_{av}(I_b)$, i.e., IVCs, at bath temperatures $T = 2.50$, 2.42, 2.31, 2.20, 2.10, 2.04, 1.99, 1.93, 1.86, 1.80, 1.75, and 1.70 K. The inset shows the scanning electron micrograph of the measured WL device. (b) Standard deviation in voltage σ_V as a function of the bias current I_b, corresponding to the IVCs in (a). Each V_{av} and σ_V data point is found from 5000 voltage samples acquired at 200-kS/s rate.

$S_V(f)$ is the spectral power averaged over about 100 time-series data. The voltage's mean and standard deviation are calculated from 5000-point voltage time series at 200 kS/s for measuring dc current-voltage characteristics of the WL. Here, we report our measurements and analysis on one WL device and a μ-SQUID while we observe the same behavior in five other WL devices. For μ-SQUID measurements, the constant offset magnetic field is provided using a superconducting electromagnet built in the closed-cycle refrigerator capable of 2-T magnetic field at 10-A current. A small low-inductance superconducting coil, closely coupled to the device [29], is used to provide the oscillating magnetic field. The maximum frequency of the oscillating magnetic field is limited to approximately 2 kHz due to eddy current heating of the metallic sample holder at higher frequencies.

V. TIME-AVERAGED WL CHARACTERISTICS AND RTN

Figure 2(a) shows the IVCs in a current range encompassing I_c and I_r^{dyn} of the studied Nb WL device for

temperatures T from 2.5 to 1.7 K. Note that both I_c and $I_r^{\rm dyn}$ change by nearly a factor of 2 over this temperature range. In this temperature range, the experimental IVCs are seen to change from smooth and reversible to hysteretic behavior. On the high-temperature side $T > T_h$ (see below), random switchings occur in the current range $I_r^{\rm dyn} < I_b < I_c$ between the zero and the finite voltage states of the WL. Here the mean interval between switches (approximately τ_i) is short compared to the voltage averaging time of 25 ms. A smooth IVC is thus observed without hysteresis, see data at 1.9 K and above. As the current bias I_b increases from $I_r^{\rm dyn}$ to I_c, the WL spends more time in the finite voltage state and thus $V_{\rm av}$ increases smoothly from zero to v.

In a narrow temperature window near the threshold temperature $T_h \sim 1.8$ K, the random switches between the zero- and finite-voltage states occur at a rate in between the voltage sampling time and the averaging time. This can be seen in Fig. 3(a) as RTN in the voltage time series taken at I_{b0}. A time series consists of discrete voltage readings taken at a 5-μs interval with each being the result of voltage sampling by the A/D card for about 2 μs, which is significantly smaller than τ_i. Given the uncorrelated nature of the switchings, from the analysis presented further, a repeat of such time series will give another realization of the set of switches. If the mean switching time is comparable to the voltage averaging time, a significant spread in $V_{\rm av}$ and σ_V will be obtained as evident in Fig. 2 for temperatures between 1.75 and 1.9 K. Such a regime of stochastic voltage response of a WL has been used to generate random numbers [37].

At lower temperature $T < T_h$ (see data at 1.7 K), a fully hysteretic IVC is observed as the switching time, again considered in the current range $I_r^{\rm dyn} < I_b < I_c$, is larger than the voltage averaging time of 25 ms. As a consequence, the dissipative state is reached at I_c and the superconducting one recovered at $I_r^{\rm dyn}$.

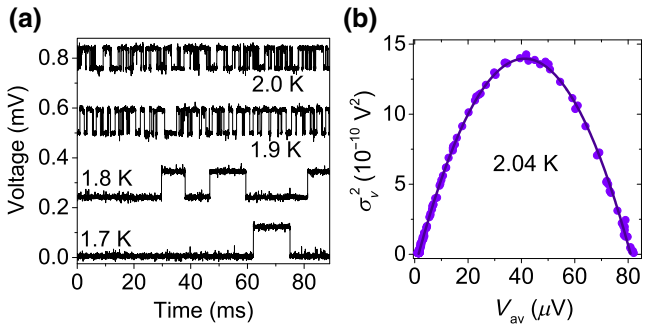

FIG. 3. (a) Time traces of the voltage signal at the symmetric bias and at different temperatures plotted with equal offsets for clarity. (b) Variance σ_V^2 versus average voltage $V_{\rm av}$ at 2.04 K with the dots as the experimental data and solid line as the fit to Eq. (1).

The criteria used for the estimation of T_h relies on the magnitude of voltage averaging time. A faster IVC measurement would have shown a transition to a hysteretic IVC at higher temperature. The definition of the threshold temperature T_h is therefore slightly measurement bandwidth dependent, in analogy to the blocking temperature in superparamagnets [38] at which a crossover from hysteretic to nonhysteretic behavior is seen.

The voltage standard deviation σ_V depends parabolically on the average voltage $V_{\rm av}$, as predicted by Eq. (1), see Fig. 3(b). The maximum of σ_V^2 occurs at the current bias point $I_b = I_{b0}$, where the RTN is symmetric with $\tau_1 = \tau_2$, $V_{\rm av} = v/2$ and $\sigma_V^2 = v^2/4$. All the noise and ac measurements are carried out at this symmetric bias current I_{b0} for ease of analysis. The two bias-current I_b values at which σ_V (due to RTN) goes to zero correspond to $I_r^{\rm dyn}$ and I_c. With increasing bath temperature T, the critical current I_c reduces and thus both the voltage v just above I_c and the variance σ_V^2 decrease. For $T > 2.2$ K, a faster decline in σ_V is observed, see Fig. 2(b), which comes from the switching rates τ_i^{-1} exceeding the voltage measurement bandwidth.

Figure 3(a) shows that the switching rates rapidly increase with increasing temperature. Consistently, the low-frequency power spectral density $S_V(f)$ decreases with increasing temperature, see Fig. 4. A Lorenzian analysis following Eq. (2) is performed, including a white-noise contribution of magnitude 12 nV/Hz and a $1/f$ noise. These extrinsic contributions arise from sources other than the WL, such as the voltage preamplifier. The $1/f$

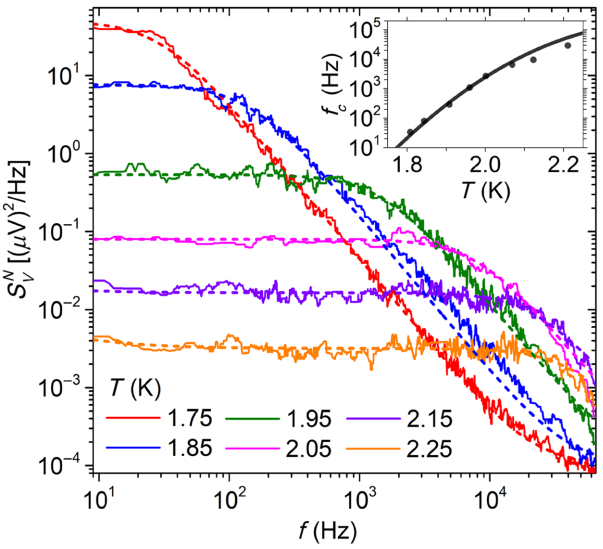

FIG. 4. Power spectral density $S_V(f)$ of the WL voltage signal at the symmetric bias point and at different temperatures. The data are shown as full lines and the corresponding Lorenzian fits are displayed as dashed lines. The inset shows the variation of f_c, obtained from the Lorenzian fits, with temperature. The data is shown with symbols and a parabolic fit by a continuous line.

component is negligible except for the highest temperatures, where it leads to a slight upturn at low frequencies. Besides these fixed extrinsic contributions, and because v is known from the σ_V^2 analysis, the cutoff frequency f_c is the only free parameter here. This, and the absence of any sharp peaks in measured $S_V(f)$, clearly establishes the RTN behavior of the voltage. Interestingly, f_c is found to rise nearly exponentially with the bath temperature T, growing by 4 orders of magnitude in a rather narrow approximately 0.5-K temperature window, see Fig. 4 inset.

VI. RESPONSE TO A PERIODIC CURRENT DRIVE AND STOCHASTIC RESONANCE

For determining the device response to a periodic current drive, we add to the current bias I_{b0} at the symmetric point a small ac current at a frequency $f_{\rm dr}$ and with a constant amplitude $\delta I_0 = 0.21\ \mu$A. The latter value is chosen to be small compared to the extent $I_c - I_r^{\rm dyn}$ of the bistable region, which secures the small perturbation limit of the stochastic resonance. The voltage response amplitude V_0 at the frequency $f_{\rm dr}$ is measured using a lock-in amplifier at different bath temperatures. The frequency response is found to follow the expected behavior of a second-order low-pass filter with a cutoff frequency f_c, see Fig. 5. The solid lines in this plot show the prediction from Eq. (4) with no fitting parameter, as both $\alpha v/2$ and f_c values at each bath temperature T are known from the preceding analysis.

The SNR is experimentally determined from the power spectral density $S_V^N(f)$ by taking the ratio of the signal power to the noise power at a fixed drive frequency [29]. Figure 5 inset shows a nearly exponential rise in SNR with temperature. The relative rise in SNR, over the same 0.5-K temperature range, is less than that of f_c as seen in the inset

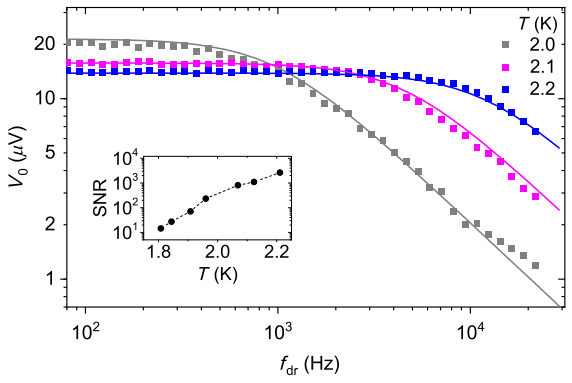

FIG. 5. Voltage response amplitude V_0 of the WL as a function of the bias drive frequency $f_{\rm dr}$ at different temperatures for a fixed ac drive amplitude $\delta I_0 = 0.21\ \mu$A at the symmetric point. The symbols are the data and the solid lines are calculated using Eq. (4). Note the logarithmic scale for both the axes. The inset shows the measured variation of SNR (at $f_{\rm dr} = 100$ Hz) with bath temperature.

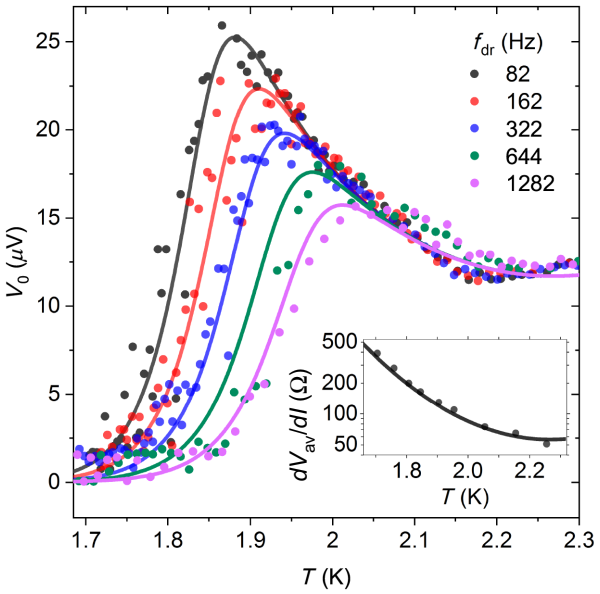

FIG. 6. Amplitude of the WL response V_0 to a periodic bias drive of amplitude 0.21 μA at the symmetric bias point as a function of the bath temperature for different drive-frequency $f_{\rm dr}$ values. The symbols are the data. The inset shows in a semilogarithmic scale the temperature dependence of the IVC slope, which is equal to $\alpha v/2$, together with a quadratic fit. This fit and that of $f_c(T)$, shown in the inset of Fig. 4, are used as the sole parameters of the main panel calculated curves (continuous lines) using Eq. (4).

of Fig. 4. This can be understood from the reduction in α with temperature, see Eq. (6).

In order to evidence the phenomenon of stochastic resonance, we show in Fig. 6 the ac response as a function of temperature and at several different drive-frequency $f_{\rm dr}$ values. The fits of $f_c(T)$ and $\alpha v/2(T)$ (solid lines in Figs. 4 and 6 insets) are used in calculating the temperature-dependent V_0, shown by continuous lines in Fig. 6 at the same $f_{\rm dr}$ values. The experimental data agree well with the calculations. From Eq. (4), we note that the initial sharp rise in V_0 with temperature comes from a nearly exponential increase in f_c while the decline beyond the peak occurs due to a reduction in $\alpha v/2$, i.e., the IVC slope. Eventually the peak occurs close to a temperature at which $f_c = f_{\rm dr}$. We note that the slope of the IVC just above I_c leads to a small variation in v at the drive frequency. This slope is less than 5% of the slope of the transition region below I_c. We ignore this small contribution to V_0 in the calculated curves, which may be responsible for the nonzero V_0 at low temperatures.

This observed behavior is qualitatively similar to the expected response in the presence of a noise intensity D depicted in Fig. 1. For most studied experimental stochastic resonance systems [3,6,10], one varies noise (D or k_BT) keeping a constant ΔU in order to analyze the response at a fixed $f_{\rm dr}$ as a function of D. This provides the most

direct evidence of stochastic resonance. In our case, the extrinsic noise of nonthermal origin is essentially constant, so that the noise amplitude is driven by temperature mainly. The thermal noise variation over a rather narrow bath-temperature range combined with the decrease of the potential barrier with temperature is enough to probe the full width of the stochastic resonance peak over a range of drive frequencies. Moreover, the measured increase in f_c and decrease in $\alpha v/2$ quantitatively capture the measured temperature dependence of ac response as arising from stochastic resonance.

VII. STOCHASTIC RESONANCE WITH A PERIODIC MAGNETIC FIELD DRIVE IN A μ-SQUID

In a μ-SQUID consisting of two parallel WLs, the magnetic flux leads to a periodic modulation in the critical current with a flux periodicity Φ_0. This effectively modulates the scaled bias current I_b/I_c that drives the SQUID behavior, as captured in the dynamic thermal model [24].

A periodic magnetic field drive is used, instead of a bias-current drive, to measure the voltage response of a μ-SQUID in its bistable region. A constant biasing magnetic field B_0 is first applied to submit the μ-SQUID to a magnetic flux of a quarter of a flux quantum Φ_0. In that case, the critical current response to the magnetic field is largest and linear. Moreover, the bias current is tuned to the symmetric point so that the IVC is also linear within a certain current range. Under these two combined conditions, the SQUID response $dV_{\rm av}/dB(T)$ can be written as $dV_{\rm av}/dI \times dI_c/dB$ for a small amplitude of magnetic field drive. A magnetic field excitation $\delta B = \delta B_0 \cos(2\pi f_{\rm dr}^B t)$ of frequency $f_{\rm dr}^B$ is applied, with a small enough amplitude to remain in the linear regime.

At a fixed drive frequency f_B, the amplitude of the voltage response $V_0^B(T)$ exhibits a peak in response at a temperature of about 4.7 K. This behavior is similar to the one observed in Fig. 6 in the WL device, and a signature of stochastic resonance. As in the WL case, the sharp rise is related to the exponential increase of the cutoff frequency f_c with the temperature. Above the peak, both $dV_{\rm av}/dI$ and dI_c/dB decrease with increasing temperature, leading to a sharper decrease in $dV_{\rm av}/dB(T)$ compared to the case of a WL device.

With increasing temperature, the voltage response keeps decreasing, see $V_0^B(T)$ in Fig. 7, while the noise power saturates to the white noise of the system. As a result, a peak in SNR is observed as shown in the inset of Fig. 7. The peak in SNR defines the best working region of the μ-SQUID. At a temperature above 5 K, a nonhysteretic regime is observed, but with a lower SNR. We also discuss in the Supplemental Material [29] that the flux sensitivity is enhanced in the bistable region, thanks to the large slope

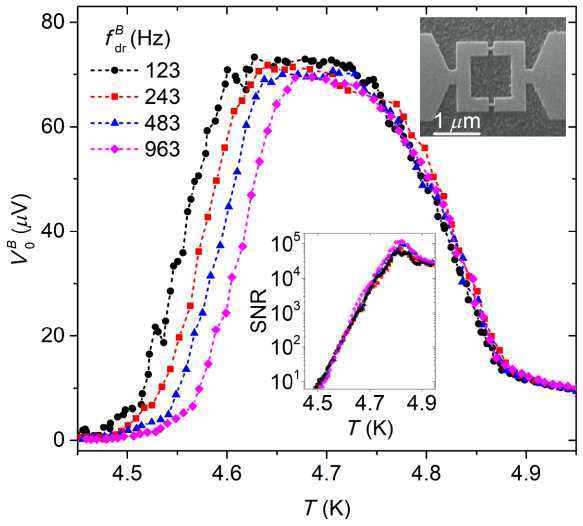

FIG. 7. Amplitude of μ-SQUID response V_0^B to a periodic magnetic field drive of amplitude 6 μT as a function of bath temperature at few different drive frequencies $f_{\rm dr}^B$. The symbols are data and the dashed lines are guiding lines. The upper inset shows the scanning electron micrograph of the measured μ-SQUID. The lower inset shows the experimentally obtained values of SNR as a function of temperature for each $f_{\rm dr}^B$.

$dV_{\rm av}/dI$ of the μ-SQUID IVC as compared to the dissipative *monostable* region [23]. The best flux resolution is found to be 10 $\mu\Phi_0/\sqrt{\rm Hz}$, which includes the magnetic field noise as there is no magnetic shield in our system.

VIII. DISCUSSION AND CONCLUSIONS

In the frame of a stochastic resonance picture, the device response to a periodic drive remains large and nearly frequency independent up to a cutoff frequency f_c. A high-f_c regime is thus preferred as it leads to higher signal-to-noise ratio and a larger measurement bandwidth. The exact optimum working parameters will also be determined by the amount of noise in the voltage signal from sources other than RTN. The crossover temperature T_h and hence the optimum working temperature can be tuned by changing the external shunt resistance and inductance [39]. A physical upper bound on the cutoff frequency f_c is set by the thermal relaxation time which sets the timescale of deterministic dynamics and eventually limits the applicability of stochastic resonance at very high frequencies.

A possible drawback of the proposed scheme for nanomagnetism studies comes from the fluctuation in WL temperature (correlated with voltage RTN), which may influence the magnetic structure. This aspect is yet to be studied in detail as it is not clear if such temperature fluctuation will be confined to the electrons of the WL or transferred to the phonons, particularly for the high-f_c regime of interest here. In the former case, a poor electronic contact of

the studied structure with the WL region may not be very difficult to achieve and enough to circumvent the issue.

In conclusion, other than illustrating the phenomenon of stochastic resonance quantitatively, our study unravels some aspects about the thermally bistable regime of a WL. The direct evidence of an enhanced SNR within the bistable region opens alternative scenarios of noise-induced improvement of the μ-SQUID performance.

ACKNOWLEDGMENTS

AKG acknowledges Sudeshna Sinha for a discussion on stochastic resonance. This work is supported by project 5804-2 from CEFIPRA, SERB-DST of the Government of India, ANR contract Optofluxonics 17-CE30-0018 and LabEx LANEF (ANR-10-LABX-51-01) project UHV-NEQ. We are indebted to Thierry Crozes for help in the device fabrication at the Nanofab platform of Néel Institute.

[1] R. Benzit, A. Sutera, and A. Vulpiani, The mechanism of stochastic resonance, J. Phys. A: Math. Gen. **14**, L453 (1981).

[2] K. Wiesenfeld and F. Moss, Stochastic resonance and the benefits of noise: From ice ages to crayfish and SQUIDs, Nature **373**, 33 (1995).

[3] S. Fauve and F. Heslot, Stochastic resonance in a bistable system, Phys. Lett. **97A**, 5 (1983).

[4] Y. Vardi, A. Guttman, and I. Bar-Joseph, Random telegraph signal in a metallic double-dot system, Nano Lett. **14**, 2794 (2014).

[5] T. Wagner, P. Talkner, J. C. Bayer, E. P. Rugeramigabo, P. Hänggi, and R. J. Haug, Quantum stochastic resonance in an ac-driven single-electron quantum dot, Nat. Phys. **15**, 330 (2019).

[6] B. McNamara, K. Wiesenfeld, and R. Roy, Observation of Stochastic Resonance in a Ring Laser, Phys. Rev. Lett. **60**, 2626 (1988).

[7] R. N. Mantegna and B. Spagnolo, Noise Enhanced Stability in an Unstable System, Phys. Rev. Lett. **76**, 563 (1996).

[8] R. L. Badzey and P. Mohanty, Coherent signal amplification in bistable nanomechanical oscillators by stochastic resonance, Nature **437**, 995 (2005).

[9] A. Simon and A. Libchaber, Escape and Synchronization of a Brownian Particle, Phys. Rev. Lett. **68**, 3375 (1992).

[10] W. Hohmann, J. Müller, and F. W. Schneider, Stochastic resonance in chemistry. 3. The minimal-bromate reaction, J. Phys. Chem. **100**, 5388 (1996).

[11] A. D. Hibbs, A. L. Singsaas, E. W. Jacobs, A. R. Bulsara, and J. J. Bekkedahl and F. Moss, Stochastic resonance in a superconducting loop with a Josephson junction, J. Appl. Phys. **77**, 2582 (1995).

[12] R. Rouse, Siyuan Han, and J. E. Lukens, Flux amplification using stochastic superconducting quantum interference devices, Appl. Phys. Lett. **66**, 108 (1995).

[13] S. Machlup, Noise in semiconductors: Spectrum of a two-parameter random signal, J. Appl. Phys. **25**, 341 (1954).

[14] H. A. Kramers, Browninan motion in a field of force and the diffusion model of chemical reactions, Physica **7**, 284 (1940).

[15] K. Murali, S. Sinha, W. L. Ditto, and A. R. Bulsara, Reliable Logic Circuit Elements That Exploit Nonlinearity in the Presence of a Noise-Floor, Phys. Rev. Lett. **102**, 104101 (2009).

[16] K. K. Likharev, Superconducting weak links, Rev. Mod. Phys. **51**, 101 (1979).

[17] F. Marsili, F. Najafi, E. Dauler, F. Bellei, X. Hu, M. Csete, R. J. Molnar, and K. K. Berggren, Single-photon detectors based on ultranarrow superconducting nanowires, Nano Lett. 11, 2048 (2011).

[18] P. Virtanen, A. Ronzani, and F. Giazotto, Josephson Photodetectors via Temperature-to-Phase Conversion, Phys. Rev. Appl. 9, 054027 (2018).

[19] W. Wernsdorfer, Classical and quantum magnetization reversal studied in nanometer-sized particles and clusters, Adv. Chem. Phys. 118, 99 (2001).

[20] D. Vasyukov, Y. Anahory, L. Embon, D. Halbertal, J. Cuppens, L. Neeman, A. Finkler, Y. Segev, Y. Myasoedov, M. L. Rappaport, M. E. Huber, and E. Zeldov, A scanning superconducting interference device with single electron spin resolution, Nat. Nanotech. 8, 639 (2013).

[21] T. Schwarz, R. Wölbing, C. F. Reiche, B. Müller, M. J. Martínez-Pérez, T. Mühl, B. Büchner, R. Kleiner, and D. Koelle: Low-Noise $YBa_2Cu_3O_7$ Nano-SQUIDs for Performing Magnetization-Reversal Measurements on Magnetic Nanoparticles, Phys. Rev. Appl. 3, 044011 (2015).

[22] N. Kumar, T. Fournier, H. Courtois, C. B. Winkelmann, and A. K. Gupta, Reversibility of Superconducting Nb Weak Links Driven by the Proximity Effect in a Quantum Interference Device, Phys. Rev. Lett. **114**, 157003 (2015).

[23] S. Biswas, C. B. Winkelmann, H. Courtois, and A. K. Gupta, Josephson coupling in the dissipative state of a thermally hysteretic micro-SQUID, Phys. Rev. B **98**, 174514 (2018).

[24] A. K. Gupta, N. Kumar, and S. Biswas, Temperature and phase dynamics in superconducting weak-link, J. Appl. Phys. **116**, 173901 (2014).

[25] W. J. Skocpol, M. R. Beasley, and M. Tinkham, Self-heating hotspots in superconducting thin-film microbridges, J. Appl. Phys. **45**, 4054 (1974).

[26] S. Biswas, N. Kumar, C. B. Winkelmann, H. Courtois, and A. K. Gupta, Random telegraphic voltage noise due to thermal bi-stability in a superconducting weak link, AIP Conf. Proc. **1731**, 130001 (2016).

[27] Note that on extremely short timescales (approximately ps) well beyond experimental bandwidth and given by the Josephson frequency, the voltage in the dissipative state is itself time dependent.

[28] For the spectral power we work in f domain, rather than ω $(= 2\pi f)$, eliminating the need for a 2π normalization factor. Further, the magnitude of spectral power does not depend on the sign of f for the real measured signals. We use a convention in which we work with only positive f with $S(f)$ values doubled to account for spectral power of negative f. The average from $V(t)$ is also subtracted out before calculating Fourier transform, which makes $S(0) = 0$. We summarize this in two relations:

$S_V(f) = 2\int_{-\infty}^{\infty} A_V(s)e^{-i2\pi fs}$ ds and total spectral power, $\int_0^{\infty} S_V(f)df = \sigma_V^2$, with $A_V(t)$ as the autocorrelation function of $V(t)$.

[29] See Supplemental Material at http://link.aps.org/supplemental/10.1103/PhysRevApplied.15.024009 for mathematical details on the two-state model of stochastic resonance and some experimental details.

[30] L. Gammaitoni, P. Hänggi, P. Jung, and F. Marchesoni, Stochastic resonance, Rev. Mod. Phys. **70**, 223 (1998).

[31] From Kramer's rate expression we see that for unequal $\omega_{1,2}$, the equality of $\tau_{1,2}$ at a particular I_b, which controls $\Delta U_{1,2}$, will also depend on the noise intensity D. Both τ_i's decrease with increasing D, following $\exp(-\Delta U_i/D)$ and for, say, $\Delta U_1 > \Delta U_2$, τ_1 will decrease faster. In other words, for an increasing D preserving the condition $\tau_1 = \tau_2$ requires simultaneously raising ΔU_1 and lowering ΔU_2, see Fig. 1 inset, which is achieved by adjusting I_b. Yet, f_c will increase with D, with a dependence in between $\exp(-\Delta U_1/D)$ and $\exp(-\Delta U_2/D)$.

[32] M. Tinkham, *Introduction to Superconductivity* (McGraw-Hill, New York, 1996), 2nd ed.

[33] H. Courtois, M. Meschke, J. T. Peltonen, and J. P. Pekola, Origin of Hysteresis in a Proximity Josephson Junction, Phys. Rev. Lett. **101**, 067002 (2008).

[34] E. Ben-Jacob, D. J. Bergman, and Z. Schuss, Thermal fluctuations and lifetime of the nonequilibrium steady state in a hysteretic Josephson junction, Phys. Rev. B 25, 519 (1982).

[35] D. Valenti, C. Guarcello, and B. Spagnolo, Switching times in long-overlap Josephson junctions subject to thermal fluctuations and non-Gaussian noise sources, Phys. Rev. B 89, 214510 (2014).

[36] N. Shah, D. Pekker, and P. M. Goldbart, Inherent Stochasticity of Superconductor-Resistor Switching Behavior in Nanowires, Phys. Rev. Lett. **101**, 207001 (2008).

[37] M. Foltyn and M. Zgirski, Gambling with Superconducting Fluctuations, Phys. Rev. Appl. **4**, 024002 (2015).

[38] C. P. Bean and J. D. Livingston, Superparamagnetism, J. Appl. Phys. **30**, 120S (1959).

[39] S. Biswas, C. B. Winkelmann, H. Courtois, and A. K. Gupta, Elimination of thermal bistability in superconducting weak-links by an inductive shunt, Phys. Rev. B **101**, 024501 (2020).